ADVANCES IN ATMOSPHERIC SCIENCES, VOL. 30, NO. 3, 2013, 699–712

# Variation of Surface Temperature during the Last Millennium in a Simulation with the FGOALS-gl Climate System Model

ZHANG Jie*[1,2,3] (张 洁), Laurent LI[2,3], ZHOU Tianjun[1] (周天军), and XIN Xiaoge[3] (辛晓歌)

[1]*State Key Laboratory of Numerical Modeling for Atmospheric Sciences and Geophysical Fluid Dynamics, Institute of Atmospheric Physics, Chinese Academy of Sciences, Beijing* 100029

[2]*Laboratoire de Météorologie Dynamique/CNRS, Université Paris* 6*, France*

[3]*National Climate Center, China Meteorological Administration, Beijing* 100081

(Received 28 July 2012; revised 22 January 2013)

**ABSTRACT**

A reasonable past millennial climate simulation relies heavily on the specified external forcings, including both natural and anthropogenic forcing agents. In this paper, we examine the surface temperature responses to specified external forcing agents in a millennium-scale transient climate simulation with the fast version of LASG IAP Flexible Global Ocean-Atmosphere-Land System model (FGOALS-gl) developed in the State Key Laboratory of Numerical Modeling for Atmospheric Sciences and Geophysical Fluid Dynamics, Institute of Atmospheric Physics (LASG/IAP). The model presents a reasonable performance in comparison with reconstructions of surface temperature. Differentiated from significant changes in the 20th century at the global scale, changes during the natural-forcing-dominant period are mainly manifested in the Northern Hemisphere. Seasonally, modeled significant changes are more pronounced during the wintertime at higher latitudes. This may be a manifestation of polar amplification associated with sea-ice–temperature positive feedback. The climate responses to total external forcings can explain about half of the climate variance during the whole millennium period, especially at decadal timescales. Surface temperature in the Antarctic shows heterogeneous and insignificant changes during the preindustrial period and the climate response to external forcings is undetectable due to the strong internal variability. The model response to specified external forcings is modulated by cloud radiative forcing (CRF). The CRF acts against the fluctuations of external forcings. Effects of clouds are manifested in shortwave radiation by changes in cloud water during the natural-forcing-dominant period, but mainly in longwave radiation by a decrease in cloud amount in the anthropogenic-forcing-dominant period.

**Key words**: last millennium, external forcing, surface temperature, cloud radiative forcing, climate system model

**Citation**: Zhang, J., L. Li, T. J. Zhou, and X. G. Xin, 2013: Variation of surface temperature during the last millennium in a simulation with the FGOALS-g1 climate system model. *Adv. Atmos. Sci.*, **30**(3), 699–712, doi: 10.1007/s00376-013-2178-0.

## 1. Introduction

Global mean surface temperature experienced an increase of about 0.74°C±0.18°C during the last century, and this global warming accelerated during the second half of the last century (IPCC, 2007). It is generally recognized that this global warming is very likely attributable to anthropogenic activities enhancing levels of greenhouse gases in the atmosphere (Tett et al., 1999; Stott et al., 2000; Tett et al., 2002). However, in the historical epoch before the industrial era, climate also experienced warm and cold periods, which are clearly not attributable to human activities. The "Medieval Climate Anomaly" (MCA; 1000 to 1300 A.D.) and "Little Ice Age" (LIA; 1400 to 1700 A.D.) are two typical periods of natural climate change in the millennial timescale before the 20th century warming period (20CW; 1900 to 1999 A.D.). Although both

*Corresponding author: ZHANG Jie, jiezhang@cma.gov.cn

the MCA and 20CW feature moderate climate conditions, temperature and hydroclimate changes in the MCA were nonuniform in comparison with the recent global warming scenario, and its warming magnitude in certain regions may have been close to, or even exceeded, that in the 20th century (e.g. Moberg et al., 2005; Mann et al., 2009; Guiot and Corona, 2010). A comparison among the three typical epochs is therefore important to understand differences between natural and human-induced climate changes, and to identify the internal and forced climate variability, as well as physical processes responsible for the anomalous spatial structures.

Reconstructions are useful to reveal basic behaviors of the historical climate. However, uncertainties in the reconstruction of existing climate should be considered. The uncertainty mainly stems from limitations in proxy data and the way they record the variables, as well as the statistical methods for the reconstruction (e.g. Mann, 2002; NRC, 2006; Jones et al., 2009). Multi-proxy reconstruction is a great approach to reconstruct large-scale surface temperature patterns, although it may be affected by various properties of the proxy sources such as the differences in major temporal climate variability (Jones et al., 2009). Recently, Mann et al. (2009) used a global climate proxy network and reconstructed surface temperature patterns over the past 1500 years.

Numerical modeling is also an important approach for paleoclimate study. It helps to provide possible climate features ignored in the reconstructions, to interpret geophysical mechanisms determining climate variation, and to identify the uncertainties in both reconstructions and simulations (e.g. Ammann et al., 2007; Zhou et al., 2009; Servonnat et al., 2010; González-Rouco et al., 2011; Goosse et al., 2011; Liu et al., 2011; Swingedouw et al., 2011). Climate models with various complexities have been used for paleoclimate studies (e.g. Crowley, 2000; Bertrand et al., 2002; Bauer et al., 2003; Goosse et al., 2013). By a model–data comparison using ensemble simulations with 25 members, Goosse et al. (2005a) demonstrated that the forced response can explain a large amount of information about the behavior of the climate system at the hemispheric scale, but the forcing has only a weak contribution compared to internal variability at regional and local scales. Simulations with the 4th version of the climate system model developed in Institute Pierre Simon Laplace (IPSL CM4) showed similar results, in that 80% of the temperature variance in the NH before 1850 A.D. can be attributed to the forced variability, dominated by solar forcing, whereas the forced variability represents at least half of the temperature signal over only about 30% of the surface of the globe (Servonnat et al., 2010).

In this paper, the climate of the last millennium is examined using the fast version of LASG IAP Flexible Global Ocean-Atmosphere-Land System model (FGOALS-gl). Previous transient and equilibrium simulations indicate that FGOALS-gl without flux adjustment can continuously run for 1000 years without significant drift and show reasonable performance in its reproduction of the MCA, LIA and 20CW (Zhang et al., 2009; Man and Zhou, 2011; Man et al., 2011; Zhou et al., 2011). Based on the 1000-yr transient simulation of FGOALS-gl, we focus on comparing the magnitude and spatial structure of temperature changes during the natural-forcing-dominant periods with that of the recent warming period, and estimating the influences of main external forcings and internal variability. The relations between surface temperature response and cloud radiative forcing are discussed. Diagnosis indicates that temperature changes in the natural-forcing-dominant periods are temporally and spatially more heterogeneous than those in the recent period. Climate responses to external forcings can explain 51.8% of the variance over the whole millennium period and mainly manifest at the decadal timescale. External forced signals in the MCA and LIA are mainly attributed to solar and volcanic forcings, explaining about 15% of the total variance. Contribution of external forcings increases up to 56.4% in the 20th century and is mainly attributed to anthropogenic factors. A negative feedback of clouds is always present in FGOALS-gl. The shortwave cloud radiative forcing (CRF) dominates during the natural-forcing-dominant periods and is associated with the cloud water path. In the 20th century, the decreasing trend in cloud cover has great impact on CRF, leading to a weakened cloud shortwave cooling and longwave warming effect.

The remainder of the paper is organized as follows. Model description and experiment design are introduced in section 2. In section 3, after model assessment, the spatiotemporal details of surface temperature and the contributions of external forcings are investigated. As important modulators of climate, the radiative effects of clouds are also discussed in section 3. Conclusions are given in section 4.

## 2. Model description and experiment design

FGOALS-gl is a climate system model developed at the LASG/IAP in China (Zhou et al., 2008). It consists of four components of the earth system: a low-resolution version of the grid-point atmospheric model developed in LASG/IAP, GAMIL (Wen et al., 2007); an oceanic component LASG/IAP Climate sys-

tem Ocean Model, LICOM (Jin et al., 1999; Liu et al., 2004); and land and sea ice components derived from the 2nd version of the Community Climate System Model developed in the National Center for Atmospheric Research, NCAR CCSM2 (Bonan et al., 2002; Briegleb et al., 2004). The atmosphere has 26 vertical levels, a model top at 2.194 hPa, and horizontal resolutions of 5°(lon)×4°(lat). The model parameters are the same as in the standard version of GAMIL, which employs a horizontal resolution of 2.815°×2.815° (Li et al., 2007). With lower atmospheric resolution, FGOALS-gl (the "l" in FGOALS-gl standing for low resolution) is suitable for long-term simulation. The ocean has a horizontal resolution of 1°×1° and 30 levels in the vertical direction. The climate sensitivity of FGOALS-gl to $CO_2$-doubling, in terms of surface temperature, is about 1.2°C, slightly lower than the IPCC range of 1.5°C–4.5°C (IPCC, 2007).

First, a 100-year spin-up run was conducted with perpetual 1000 A.D. external forcing agents. The oceanic initial state was derived from another 500-yr spin-up integration, but with present-day conditions

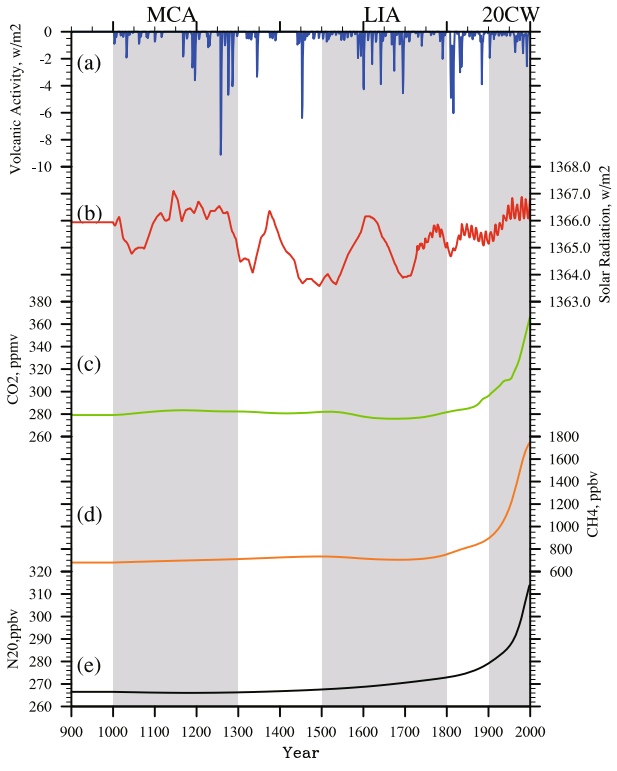


**Fig. 1.** Time series of the external forcings: (a) volcanic eruptions (W $m^{-2}$); (b) solar irradiation (W $m^{-2}$); (c) $CO_2$ (ppmv); (d) $CH_4$ (ppbv); (e) $N_2O$ (ppbv). Perpetual 1000 A.D. external forcings were used in the spin-up period from 900–1000 A.D. The shading indicates the three typical periods: MCA; LIA; 20CW.

(Liu et al., 2004). The 100-year simulation continued for a further 1000 years, incorporating year-to-year changes in solar irradiation, volcanic eruptions, as well as greenhouse gas concentrations. The individual forcing factor was the same as that in Peng et al. (2009) and is described in Fig. 1. Both volcanic (Fig. 1a) and solar (Fig. 1b) forcing series were derived from Crowley et al. (2003). The solar forcing increased by about 1.98 W $m^{-2}$ from the Maunder Minimum (1647–1715 A.D.) to the present day value, larger than recent evaluations (0.9±0.4 W $m^{-2}$) (Tapping et al., 2007; Steinhilber et al., 2009; Schmidt et al., 2011). The comparatively high solar variability may have exaggerated its climate influence in our simulation. Changes in greenhouse gas concentrations (Figs. 1c–e), i.e. $CO_2$, $CH_4$, and $N_2O$, were the same as in Ammann et al. (2007). Anthropogenic tropospheric sulphate aerosols forcing was taken into account from 1850 A.D.

## 3. Changes in surface temperature

### 3.1 *Model assessments: Annual mean evolutions*

Based on 39 individual proxies in 30 distinct regions, Wang et al. (2002; hereafter referred to as WSW2002) reconstructed the surface temperature (TS) series in both the Northern (20 sites) and Southern (10 sites) Hemispheres. The geographic distributions of the proxy sites can be found in Fig. 1 of Zhang et al. (2009). All the proxy indicators are available for more than 900 years. A 50-yr running mean was applied to the original series at a high temporal resolution. Finally, all the series were transformed to a uniform structure, from 1000 A.D. to 2000 A.D. with 25-yr intervals. As shown in Zhang et al. (2009) and other recent works employing WSW2002, this compilation is a reliable dataset and has a good spatial coverage. WSW2002 is thus used in the present paper to study climate variation during the last millennium and to evaluate the performance of the model.

Results from WSW2002 and our simulation are shown in Fig. 2. The time series were smoothed with a 30-yr filter and scaled to have zero mean over the period 1500 A.D. to 1899 A.D. In the NH (NH; Fig. 2a), warm anomalies at the beginning and end of the last millennium, as well as cool anomalies in the intermediate period, are visible in both WSW2002 (black line) and the simulation (blue line). The simulation shows a NH temperature evolution comparable to the WSW2002 reconstruction. The solar minima — Spörer (1450–1540 A.D.), Maunder (1645–1715 A.D.) and Dalton (1790–1820 A.D.) — are clearly visible in the simulation. The difference at the beginning of the millennium may be partly due to initial conditions

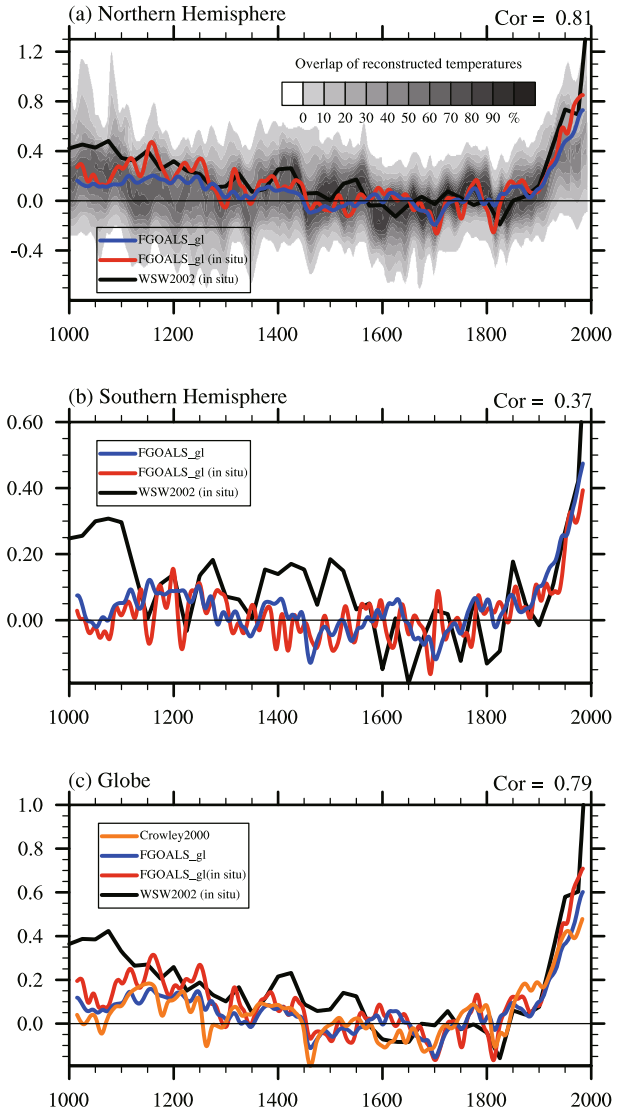


**Fig. 2.** Annual mean surface temperature anomalies relevant to the 1500–1899 A.D. means in the (a) NH; (b) SH. (c) The same as (a) and (b), but for global mean results. The black line represents the reconstruction WSW2002. The red and blue lines represent the associated simulations calculated by the in situ and area-mean surface temperature, respectively. The correlation coefficient between the simulated in situ mean surface temperature and the reconstruction WSW2002 is marked at the top-right corner of each panel. The gray shadings in (a) describe the overlap of the uncertainty ranges of NH reconstructions, as in the Figure 6.13d of IPCC AR4 (Jansen et al., 2007). . The orange line in (c) is derived from an energy balance model (Crowley, 2000). Fluctuations at time scales less than 30 years have been removed.

and model sensitivity, as well as uncertainties in both surface temperature and external forcing reconstructions (e.g. Goosse et al., 2005b).

The background shading in Fig. 2a represents the concentration of overlapping NH reconstructions, and the uncertainties are large at the beginning of the millennium. The decreasing availability of proxy sources and the deterioration of some proxy data back through time may be responsible for the inter-reconstruction variability. The uncertainties in the reconstruction can also be attributed to the relatively short length of instrumental data for calibrating and validating the reconstructions, as well as the uncertainties associated with the methods used to carry out the reconstructions. Generally speaking, both the simulation and WSW2002 show agreement with previous reconstructions. For the SH (Fig. 2b), the amplitude of the anomalies is smaller than that in the NH. This is due to its dominant oceanic coverage.

Differences between WSW2002 and the simulation may be partly attributable to the limited number and spatial position of proxy sites. For a more appropriate comparison, the simulated hemispheric and global mean surface temperature evolutions were also calculated by the in situ mean TS across the 30 proxy sites (red lines), as in WSW2002. Compared with the reconstruction, the simulation seems fair both at global and hemispheric scales. The coherence in evolution between the reconstruction and simulation is more satisfactory for the NH, with a correlation coefficient of 0.81, compared to the SH (0.37). The station-based and area-averaged TS changes in the simulation also show better agreement in the NH compared to the SH, especially in the pre-industrial era. This demonstrates that the external forcings in the simulation may have more influence on the temperature variability in the NH than in the SH.

Owing to the low sensitivity of the model, the simulated TS rises by about 0.5°C during the last century, slightly less than the IPCC range (0.74°C ±0.18°C). The simulation by an energy balance model in Crowley (2000) is shown in Fig. 2c (orange line). Similar amplitudes of temperature evolution can be seen in the models of different complexity. The correlation coefficient between the EBM and FGOALS-gl is up to 0.86. However, as a climate system model, FGOALS-gl is able to describe the spatial distributions of the climate response and allows us to better understand and identify the complex response and feedback processes in the climate system.

### 3.2 *Spatial changes of annual mean surface temperature*

Natural and anthropogenic forcings can both exert impacts on climate. However, the involved physical processes are not totally the same, which may induce subtle differences of climate response, in particular in terms of spatial distribution. In this consideration,

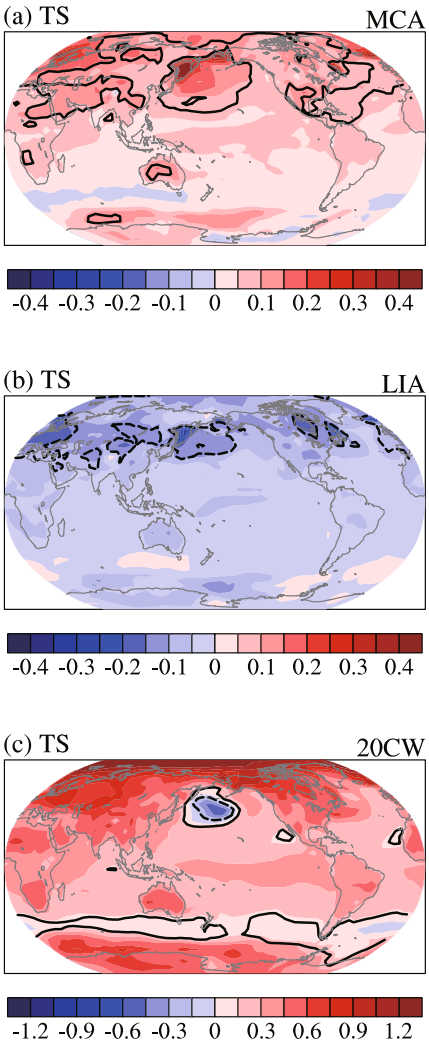


**Fig. 3.** Spatial surface temperature anomalies relevant to the 1000–1800 A.D. means: (a) MCA; (b) LIA; (c) 20CW. Units: K. Values statistically significant at the 5% level according to the Student's $t$-test are encircled by black lines. The number of degrees of freedom was estimated by testing the lag-one auto-correlation coefficient.

three typical periods are defined by the phases and types of external forcings for spatial examinations: MCA (1000–1300 A.D.); LIA (1400–1700 A.D.); and 20CW (1900–1999 A.D.). The first two periods are referred to as natural periods, with climate variation generally in relation to natural factors. All anomalies were calculated as differences to the climatology of 1000–1800 A.D.

The annual mean TS anomalies are shown in Fig. 3 for each period. Differences are clearly apparent in both magnitude and spatial structures of the anomalies. Global warming signals dominate in the 20th century (Fig. 3c), whereas changes in the natural periods are smaller in magnitude and significant changes concentrate towards higher latitudes of the NH (Figs. 3a and b). The warming in the MCA is about 0.06 K as global mean, and 0.09 K as NH mean. The LIA, however, features a cooling of 0.05 K as global mean and 0.07 K as NH mean.

In the reconstructions, a distinct climate shift from the MCA to LIA is characterized by more La Niña-like states during the Medieval Period (Cobb et al., 2003; Graham et al., 2007; Mann et al., 2009). Fossil-coral records from the central tropical Pacific document a broad range of ENSO behavior during the last millennium (Cobb et al., 2003), but the ENSO behavior cannot be explained by changes in the mean state or noise in the climate system and the majority of ENSO variability may arise from dynamics internal to the climate system. The effects of external forcings may also play a role. Adams et al. (2003) suggested that volcanic forcing drives the climate system more subtly towards an El Niño-like state. Using a climate model of intermediate complexity (EMIC) — the Cane-Zebiak model of tropical Pacific coupled ocean–atmosphere dynamics (Zebiak and Cane, 1987) — Emile-Geay et al. (2007) found an almost linearly intensified response of the zonal SST gradient along the tropical Pacific Ocean to increased solar forcing. They indicated that the increased SST gradient in response to positive radiative forcing may be associated with the strong upwelling and surface divergence in the eastern tropical Pacific, which transports some of the radiative heating poleward. The SST gradient will strengthen and sustain based upon the Bjerknes positive feedback process of tropical ocean-atmosphere interaction (Bjerknes, 1969). It is worth noting that the Cane-Zebiak model has stronger dynamical feedback than most global models and the responses all arise from intrinsic tropical Pacific climate mechanisms.

Considering the limitations of EMICs, in that they can lack some important features and do not have a fine enough spatial resolution, comprehensive global coupled climate system models are more appropriate for examining the response of the tropical Pacific. However, as shown in Figs. 3a and b, the tropical SST anomalies in the MCA and LIA are insignificant in the present simulation. We also examined simulations of the last millennium in five state-of-the-art climate system models participating in Coupled Model Intercomparison Project Phase 5 (CMIP5): the version 1.1 of the climate system model developed in Beijing Climate Center, BCC-CSM1-1 (Xin et al., 2013; Wu et al., 2013) the 4th version of the Community Climate System Model developed in the National Center for Atmospheric Research, CCSM4 (Gent et al., 2011); the Commonwealth Scientific and Industrial Research Or-

ganisation (CSIRO) Mark 3 reduced-resolution model version 1.2, CSIRO-Mk3L-1-2 (Phipps, 2010); the climate system model developed in Goddard Institute for Space Studies (GISS), GISS-E2-R (Schmidt et al., 2006); and the Earth system model of the Max Planck Institute, MPI-ESM-P (Raddatz et al., 2007). None of these models can significantly reproduce the El Niño/La Niña tendency discovered in reconstructions and the changes in the tropical Pacific (data not shown). Despite recent progress in the understanding of the ENSO phenomenon, many aspect of its physics remain unknown, such as the origin of ENSO's observed irregularity. The oceanic modules of recent climate system models can lack some of the important features that may be responsible for the missing El Niño/La Niña tendencies in their simulations. Therefore, physical processes in the oceanic modules of recent climate system models need further improvements to obtain realistic responses to external forcing in the tropical Pacific.

The insignificant tropical response in climate system models may also be partly attributable to the strength of external forcing. The amplitudes of variability in the recommended CMIP5 solar forcing series (expressed as difference between the present day value and the Maunder Minimum) is less than 0.1%. In the case of the Cane-Zebiak model, solar forcing increasing by about 0.2% is sufficient to trigger the tropical Pacific feedbacks, while the 0.05% case is insufficient (Emile-Geay et al., 2007).

An interesting feature is the opposite surface temperature anomalies in the North Pacific in the two warm periods: warming in the MCA but cooling in 20CW. Surface temperature anomalies lead to the changes in temperature stratification and vertical motions, and affect the large-scale circulation with significant regional climate effects. The cooling/warming anomalies correspond to a stronger/weaker Aleutian Low in the 20th Century/MCA. A North Pacific cooling trend for the second half of the 20th century was also evident in the simulations using the Geophysical Fluid Dynamics Laboratory Coupled Model version 2 (GFDL CM2) and FGOALS-gl (Knutson et al., 2006; Man et al., 2011), consistent with observational evidence. Deser and Phillips (2009) stated that the intensification of the Aleutian Low can be attributed to tropical oceanic forcing and the direct atmospheric radiative forcing tends to partly offset the deepening of the Aleutian Low. However, as shown in Figs. 3a and c, structures of the tropical SST anomalies in the MCA and 20CW are similar and the changes in the MCA are insignificant. The opposite surface temperature anomalies in the North Pacific in the MCA and 20CW, at least in the present model, cannot be well explained by changes in the tropical Pacific. The surface temperature changes in the MCA/20CW may partly be attributable to the weak/strong cloud shortwave radiative cooling anomalies over the North Pacific in association with the changes of low-level cloud amounts (data not shown).

### 3.3 *Seasonal changes*

Changes in surface temperature changes are also visible at seasonal timescales. Figure 4 presents latitude–month (annual cycle) diagrams of zonal mean TS anomalies in the MCA, LIA and 20CW. As with the annual mean, TS changes skew significantly towards the NH in the MCA (Fig. 4a) and LIA (Fig. 4b), but 20CW (Fig. 4c) also has a strong warming in the Antarctic. Significant anomalies are more pronounced in the winter hemispheres, i.e. October to March

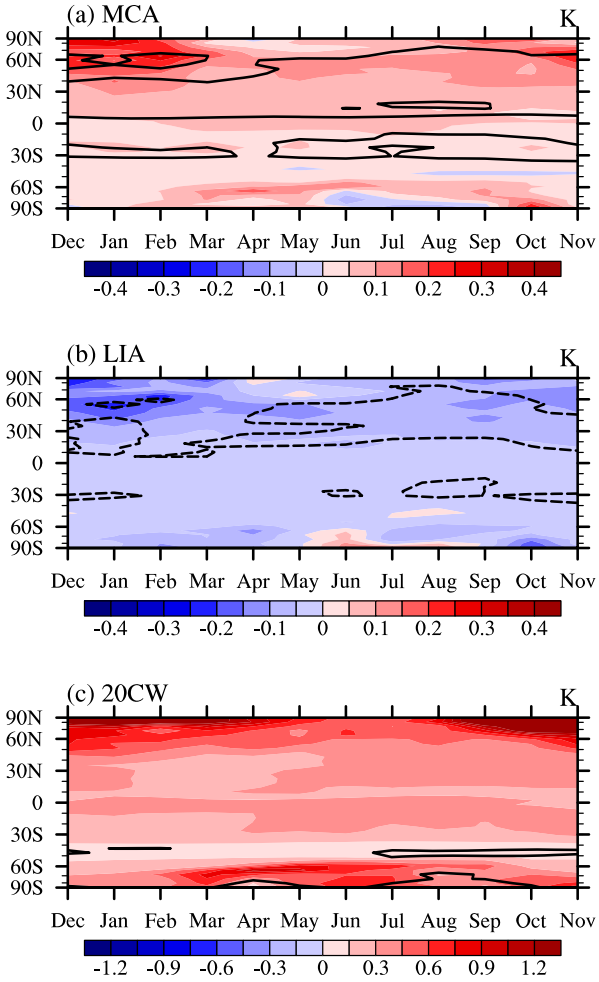


**Fig. 4.** Latitude–month sections of zonal average surface temperature anomalies in the three typical periods, relative to the 1000–1800 A.D. means. Units: K. Values statistically significant at the 5% level according to the Student's $t$-test are encircled by black lines.

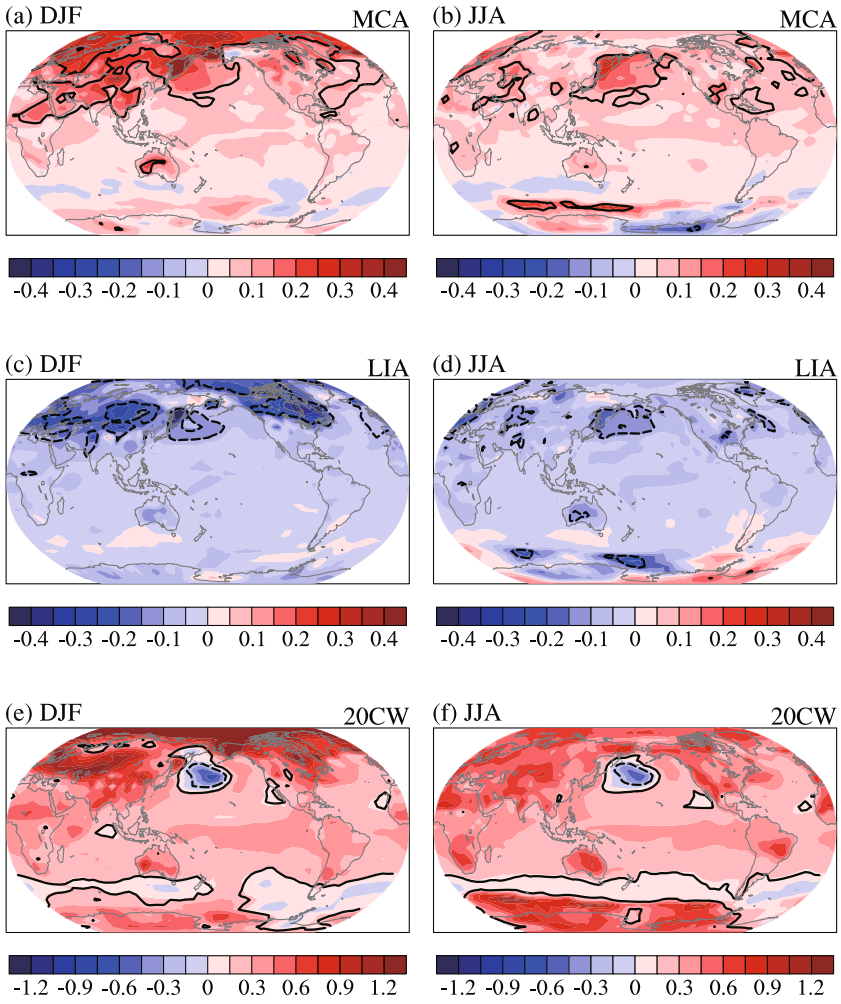


**Fig. 5.** The same as Fig. 3, but for the anomalies in DJF (left column) and JJA (right column): (a, b) MCA; (c, d) LIA; (e, f) 20CW. Units: K. Values statistically significant at the 5% level according to the Student's $t$-test are encircled by black lines.

(ONDJFM) in the NH in both the natural and anthropogenic periods, and April to September (AMJJAS) in the SH in the 20th century.

To better describe the spatial changes, Fig. 5 presents anomalous TS maps for December–January–February (DJF) and June–July–August (JJA) in each period. The all-year-round North Pacific cooling and strong warming over Antarctica in the 20th century (Figs. 5e and f) is consistent with recent assessments (Knutson et al., 2006; Steig et al., 2009). In the MCA (Figs. 5a and b) and LIA (Figs. 5c and d), the TS changes are more pronounced at mid and high latitudes during the northern winter (DJF), especially in the polar region, but the summertime changes are much smaller, with statistically significant signals in the North Pacific. In the 20th century (Figs. 5e and f), the land surface temperature warming dominates throughout the year. The warming amplitude is larger during the wintertime both for the NH (DJF) and SH (JJA). The seasonal changes may be a manifestation of polar amplification, with strong sea-ice-cover–temperature positive feedback being the major driver. Excess heat related to declines in sea ice during summer will be stored in the upper ocean and then released to the atmosphere during the following winter (Screen and Simmonds, 2010).

### 3.4 *A detection and attribution study*

In this subsection, we try to detect and estimate fingerprints of natural and anthropogenic forcings, using a statistical method based on a linear decomposition of the surface temperature anomalies as the sum of the contributions of external forcings and an associated residual noise. The method was also used by

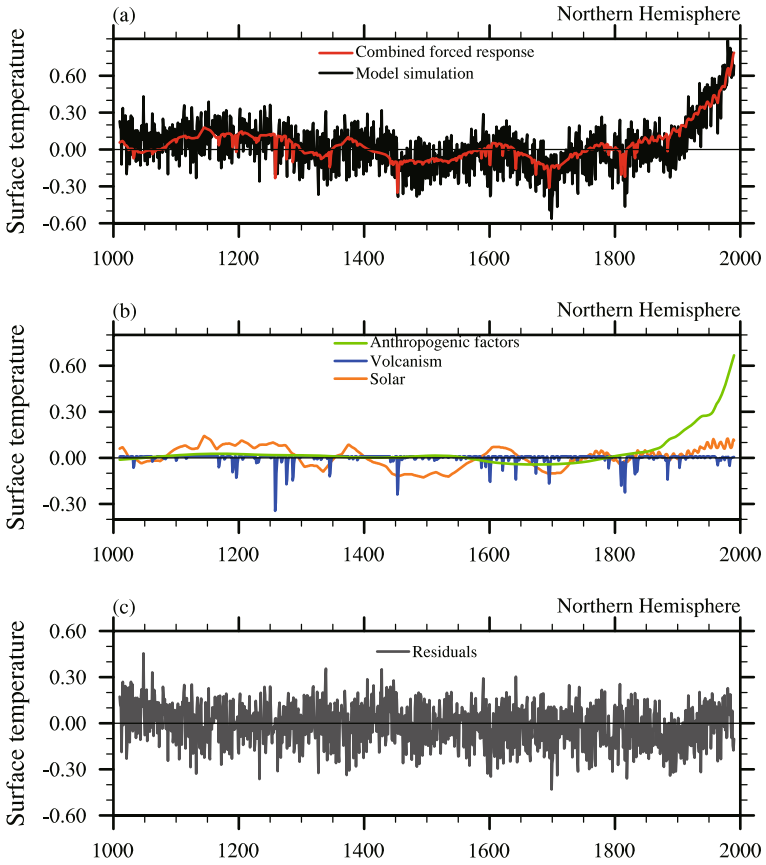


**Fig. 6.** Detection results for the simulated NH annual mean temperature anomalies relevant to 1000–1800 A.D. (a) Simulation (black line) and the best estimate of the combined forced response (red). (b) Response attributed to individual forcings: solar irradiation (orange); volcanic eruptions (blue); anthropogenic factors (green). (c) Residual variability attributed to internal climate variability. Units: K.

Servonnat et al. (2010) to examine the influence of external forcings in the IPSL CM4 model. The residual between the simulation and composition of all external forced signals is attributed to internal climate variability. Results for the NH surface temperature changes are shown in Fig. 6 and Table 1. The fingerprint of the total external forcings generally follows the evolution of NH surface temperature anomalies ($T'$), explaining 51.8% of the total variances (Fig. 6a). The separate signatures (Fig. 6b) indicate the major contributions of solar (16.8%) and anthropogenic forcing (32.5%). However, in reconstruction-based studies, a response to solar forcing cannot be robustly detected (Hegerl et al., 2003, 2007). As mentioned in section 2, the amplitude of the variability of the solar irradiation forcing is large in the present simulation and its contribution may be overestimated.

As described in Table 1, fingerprints of solar and volcanic forcings are responsible for the major external forcing response of the climate system in the MCA

**Table 1.** Variances of the NH temperature explained by total external forcings, solar irradiance, volcanic eruption and anthropogenic factors on the whole period (LM), MCA, LIA, and 20CW, units: %. Results for the decadal variances are shown in the corresponding parentheses.

| | LM | MCA | LIA | 20CW |
|---|---|---|---|---|
| Total forcings | 51.8 (85.5) | 13.3 (67.5) | 16.2 (53.9) | 56.4 (74.9) |
| Solar irradiation | 16.8 (28.3) | 6.1 (39.3) | 11.3 (43.0) | 10.5 (14.0) |
| Volcanic eruption | 2.4 (2.5) | 6.5 (23.2) | 4.6 (10.1) | −0.3 (−0.8) |
| Anthropogenic factors | 32.5 (54.6) | 0.7 (5.0) | 0.3 (0.8) | 46.2 (61.8) |

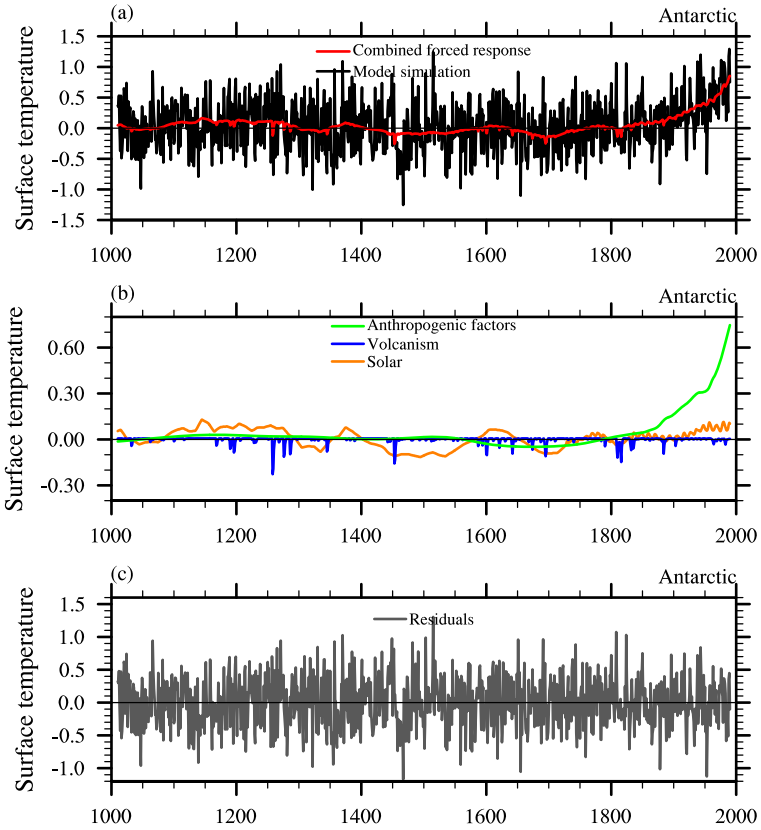


**Fig. 7.** The same as Fig. 6, but for the fingerprints of external forcings and internal variability in the Antarctic (south of 60°S).

(12.6% in 13.3%) and LIA (15.9% in 16.2%), whereas the anthropogenic warming in the 20th century is mainly attributed to increasing concentrations of greenhouse gases in the simulation (46.2% in 56.4%). Repeated examinations on decadal variance demonstrate that the contribution of external forcings mainly manifests at the decadal timescale, which is in agreement with the reconstruction study by Hegerl et al., 2007. External forcings can explain 85.5% of the decadal variance over the whole millennium period. Internal climate variability in the simulation is dominated by high frequency aspects of the signals with a standard deviation of 0.14 (Fig. 6c).

Recent assessments of Antarctic temperature reveal a warming trend in the Antarctic Peninsula, West Antarctica, as well as East Antarctica at the continent-wide scale during the last few decades (Steig et al., 2009). However, shallow marine and coastal terrestrial records along the East Antarctic coastal margin indicates that there is no evidence for a coeval Medieval Warm Period (MWP) and only weak circumstantial evidence can be found in a few places for a cool event crudely equivalent in time to the NH's LIA (Verleyen et al., 2011). The present model results also indicate heterogeneous and small TS changes in the Antarctic (Figs. 3a and b). The irregularity may be due to the internal variability in the climate system. To clarify this, we repeated the detection and attribution analysis in the Antarctic (Figs. 7 and Table 2). Different from that in the NH, internal variability is much stronger in the polar region and the standard deviation reaches up to 0.37 (Fig. 7c). The fingerprint

**Table 2.** The same as Table 1, but for variances in the Antarctic.

| | LM | MCA | LIA | 20CW |
|---|---|---|---|---|
| Total forcings | 13.7 (41.7) | 2.3 (8.1) | 2.2 (7.4) | 22.4 (50.7) |
| Solar irradiation | 3.7 (11.3) | 1.6 (7.0) | 1.9 (6.7) | 3.6 (7.6) |
| Volcanic eruption | 0.3 (0.3) | 0.5 (0.3) | 0.1 (0.2) | −0.4 (−0.8) |
| Anthropogenic factors | 9.8 (30.2) | 0.2 (0.9) | 0.2 (0.5) | 19.3 (43.9) |

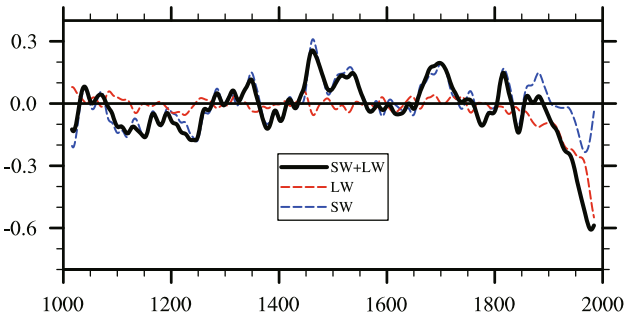


**Fig. 8.** Changes in global mean CRF relative to the 1000–1800 A.D. means: shortwave CRF (blue dashed line); longwave CRF (red dashed line); net CRF (black solid line). Positive values indicate a downward flux. Units: W $m^{-2}$.

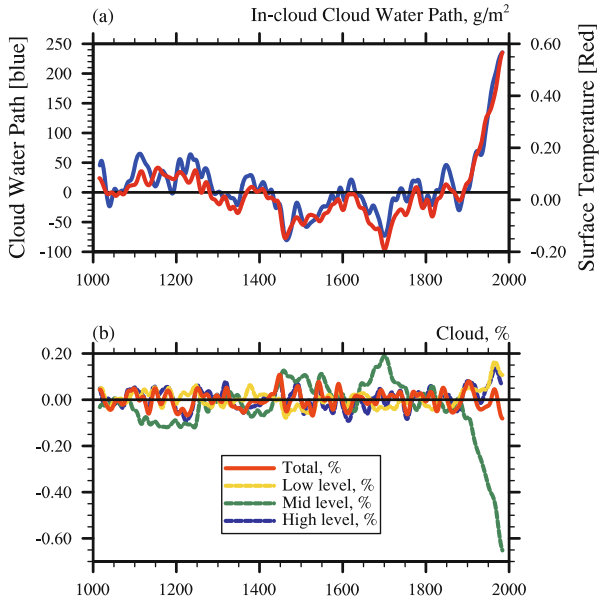


**Fig. 9.** Time series of the anomalous (a) vertical integrated in-cloud cloud water path (blue solid line; g $m^{-2}$) and (b) cloud amount at different levels (%), relative to the 1000–1800 A.D. means. Evolution of global mean surface temperature anomalies is shown by the red solid line in (a) (units: K).

of the total external forcings can only explain 13.7% of the total variances for the whole period and is mostly attributable to the strong anthropogenic warming effects in the 20th century. Signatures of external forcings are barely detected in the MCA (2.3%) and LIA (2.2%). Li and Conil (2003) indicated that the SST changes south of 30°S are closely related to the strong natural variability of the deep convection in the Southern Ocean.

### 3.5 *The possible effects of cloud radiative forcing*

In our simulation of the last millennium, major effects of natural and anthropogenic forcings operate in shortwave and longwave radiation, respectively. Such a difference is possibly thought to activate different feedback mechanisms that can amplify (positive feedback) or dampen (negative feedback) the effect of external forcing. Here, we investigate the role that a change in cloud properties can play. We study in particular how the role of clouds may change in the function of external forcing, natural or anthropogenic.

The radiative interaction between clouds and external perturbation can modulate the Earth's energy budget by reflecting parts of the shortwave radiation to space (cooling effect) and affecting the atmospheric emission of longwave radiation (positive greenhouse effect). The CRF is defined as the difference in radiative flux at the top-of-atmosphere under cloud and cloud-free conditions.

The time series of global-mean CRF are shown in Fig. 8. The net CRF (black curve) tends to suppress the climate changes. The decomposition of the net CRF into shortwave (blue dashed line) and longwave (red dashed line) components is different between the natural-forcing-dominant and anthropogenic-forcing-dominant periods. In the MCA, the CRF cooling effect prevails ($-0.066$ W $m^{-2}$) and is mostly attributed to the shortwave CRF ($-0.069$ W $m^{-2}$). Changes in the LIA show similar features as those in the MCA, but with opposite signs (0.060 W $m^{-2}$ in the shortwave CRF; 0.059 W $m^{-2}$ in the net CRF). In the instrumental epoch, CRF cooling dominates with a strongly suppressed longwave CRF warming effect. Generally, CRF acts against the fluctuations of external forcings, modulating the incoming solar radiation by cloud reflection (shortwave CRF), especially in the pre-industrial era and suppressing its longwave trapping effect (longwave CRF) afterward.

Slight changes in cloud properties have great impacts on CRF. Shortwave CRF is closely linked with the cloud water path. An increase in cloud water path leads to optically thicker clouds, and vice versa (Lee et al., 1997). As shown in Fig. 9a, the cloud water path follows the changes in temperature. As a consequence, a relatively thick (or thin) cloud optical depth results in a stronger (or weaker) negative cloud shortwave feedback in the MCA (or LIA). However, with an increase in cloud water path, a weakened rather than enhanced negative shortwave CRF is found in the second half of the 20th century. To better clarify these

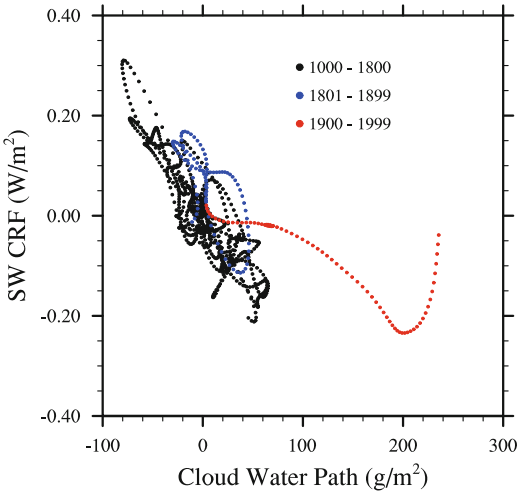


**Fig. 10.** Scatter plot of the in-cloud water path (the abscissa; g m$^{-2}$) versus the shortwave CRF (the ordinate; W m$^{-2}$). Each dot represents the values in one year. The colors of the dots stand for the values in different periods as described in the legend.

features, scatterplots for cloud water path (the abscissa) versus shortwave CRF (the ordinate) are shown in Fig. 10. The values in different epochs are classified by different colors. Negative correlation is evident in the natural-forcing-dominant periods. However, this negative correlation weakens at the beginning of the 20th century and turns to positive values in the last few decades.

The unique feature in the 20th century may be due to the changes in cloud amount. Figure 9b plots the variation of cloud amounts (low, middle, high and total). In pre-industrial times, the fluctuation of cloud amounts at different levels is approximately 0.2%. In the 20th century, the mid-level cloud amount decreases significantly. Under the conditions of decreasing cloudiness, especially in the second half of the last century when the low- and high-level cloudiness also shows a decreasing trend, the cloud shortwave reflection and longwave trapping effects are diminished. This is consistent with Quaas et al. (2004) who, using an atmospheric general circulation model, also found weakened cloud shortwave cooling and greenhouse warming under the scenario of increasing greenhouse gas concentrations. However, it should be noted that cloud observational data have only been available for the last few decades. Although satellite and surface observations indicate a reduction in high cloud cover during the 1990s relative to the 1980s, the decadal trends are substantially uncertain (Norris, 2005; IPCC, 2007).

Cloud properties show large spatial variation, with different climate effects (Kiehl, 1994; Arking and Ziskin, 1994; Philander et al., 1996; Yu et al., 1999). However, patterns of the anomalies in the MCA and LIA show almost no statistically significant signals (data not shown), indicating a strong internal variability at regional scales.

It should be noted that there is great uncertainty in cloud model data, and there are also no CRF reconstruction data available that can be compared with simulations. Our results only suggest a possible influence of the effect of CRF on the climate of the last millennium. Simulations of the climate of the last millenium in CMIP5 have already been published. For future work, a multi-model comparison could provide a more complete assessment of this aspect of the climate of the last millennium.

## 4. Conclusions

In this paper, results from a transient simulation with the climate system model FGOALS-gl have been analyzed to better understand the natural and anthropogenic climate changes that have taken place during the last millennium. Validation of model performance indicated that the model can capture well the three typical periods, i.e. the MCA, LIA and 20th century global warming. Significant surface temperature anomalies in the pre-industrial era were evident in the NH, whereas the warming anomalies in the 20th century were globally significant. The seasonal patterns of temperature changes in all the three typical periods featured a polar amplification structure and the changes were more pronounced in the winter hemispheres.

Detection and attribution analysis indicated that external forcings can explain a substantial fraction of the NH surface temperature variance in the past millennium (51.8%), especially at decadal timescales. Climate response to external forcings was mainly attributed to solar and volcanic forcings in the MCA and LIA, and dominated by anthropogenic forcings in the 20th century. Variability internal to the climate system is also important, especially at regional scales. Over the Antarctic, the model simulated heterogeneous and irregular changes in the pre-industrial era. Internal variability was strong in the Antarctic and the climate response to external forcings was barely detected before the industrial era.

Climate was affected by external forcings, but also modulated by CRF, which tended to dampen the climate response to external forcings. Its shortwave component was primarily dependent on cloud water path changes and showed its dominance before the industrial era. CRF, especially the longwave component, tended to suppress the anthropogenic warming in the

20th century.

González-Rouco et al. (2011) found large spatial discrepancies in inter-model and model/reconstruction comparisons. This indicates that the large influence of internal variability on the MCA–LIA changes or the state-of-the-art atmosphere-ocean coupled general circulation models fail to correctly reproduce the climate response to external forcings. As pointed out by Goosse et al. (2005b), model sensitivities may be responsible for many behaviors of last-millennium climate simulation. Therefore, it should be kept in mind that the results presented in this paper may depend on specific formulation and physical parameterizations employed in FGOALS-gl. In the future, we plan to use the new version of FGOALS and extend our analysis to other models providing last-millennium results under the framework of CMIP5 and the Paleoclimate Modelling Intercomparison Project phase 3(PMIP3). The current results will serve as a useful reference for comparison.

***Acknowledgements.*** This work was supported by the Major State Basic Research Development Program of China (973 Program) under Grant No. 2010CB951903, and the National Natural Science Foundation of China under Grant Nos. 40890054, 41205043, and 41105054.

## REFERENCES

Adams, J. B., M. E. Mann, and C. M. Ammann, 2003: Proxy evidence for an El Niño-like response to volcanic forcing. *Nature*, **426**(6964), 274–278.

Ammann, C. M., F. Joos, D. S. Schimel, B. L. Otto-Bliesner, and R. A. Tomas, 2007: Solar influence on climate during the past millennium: Results from transient simulations with the NCAR climate system model. *Proc. the National Academy of Sciences*, **104**(10), 3713–3718.

Arking, A., and D. Ziskin, 1994: Relationship between clouds and sea-surface temperatures in the western tropical pacific. *J. Climate*, **7**(6), 988–1000.

Bauer, E., M. Claussen, V. Brovkin, and A. Huenerbein, 2003: Assessing climate forcings of the Earth system for the past millennium. *Geophys. Res. Lett.*, **30**(6), 1276–1279.

Bertrand, C., M. F. Loutre, M. Crucifix, and A. Berger, 2002: Climate of the last millennium: A sensitivity study. *Tellus* (*A*), **54**(3), 221–244.

Bjerknes, J., 1969: Atmospheric teleconnections from the equatorial Pacific. *Mon. Wea. Rev.*, **97**, 163–172.

Bonan, G. B., K. W. Oleson, M. Vertenstein, S. Levis, X. B. Zeng, Y. J. Dai, R. E. Dickinson, and Z. L. Yang, 2002: The land surface climatology of the community land model coupled to the NCAR community climate model. *J. Climate*, **15**(22), 3123–3149.

Briegleb, B., C. Bitz, E. Hunke, W. Lipscomb, M. Holland, J. Schramm, and R. Moritz. 2004: Scientific description of the sea ice component in the community climate system model, version three. NCAR Tech. Note NCAR/TN-463+STR, National Center for Atmospheric Research, Boulder, CO, 78pp.

Cobb, K. M., C. D. Charles, H. Cheng, and R. L. Edwards, 2003: El Niño/Southern Oscillation and tropical Pacific climate during the last millennium. *Nature*, **424**(6946), 271–276.

Crowley, T. J., 2000: Causes of climate change over the past 1000 years. *Science*, **289**(5477), 270–277.

Crowley, T. J., S. K. Baum, K. Y. Kim, G. C. Hegerl, and W. T. Hyde, 2003: Modeling ocean heat content changes during the last millennium. *Geophys. Res. Lett.*, **30**(18), doi: 10.1029/2003GL017801.

Deser, C., and A. S. Phillips, 2009: Atmospheric circulation trends, 1950–2000: The relative roles of sea surface temperature forcing and direct atmospheric radiative forcing. *J. Climate*, **22**(2), 396–413.

Emile-Geay, J., M. Cane, R. Seager, A. Kaplan, and P. Almasi, 2007: El Niño as a mediator of the solar influence on climate. *Paleoceanography*, **22**(3), doi: 10.1029/2006PA001304.

Gent, P., and Coauthors, 2011: The community climate system model version 4. *J. Climate*, **24**, 4973–4991.

González-Rouco, F. J., and Coauthors, 2011: Medieval climate anomaly to little ice age transition as simulated by current climate models. *Medieval Climate Anomaly*, *Pages News*, **19**(1), 7–8.

Goosse, H., H. Renssen, A. Timmermann, and R. S. Bradley, 2005a: Internal and forced climate variability during the last millennium: A model-data comparison using ensemble simulations. *Quaternary Science Reviews*, **24**(12–13), 1345–1360.

Goosse, H., T. J. Crowley, E. Zorita, C. M. Ammann, H. Renssen, and E. Driesschaert, 2005b: Modelling the climate of the last millennium: What causes the differences between simulations? *Geophys. Res. Lett.*, **32**, L06710, doi: 10.1029/2005GL022368.

Goosse, H., J. Guiot, M. E. Mann, S. Dubinkina, and Y. Sallaz-Damaz, 2011: The medieval climate anomaly in Europe: Comparison of the summer and annual mean signals in two reconstructions and in simulations with data assimilation. *Global and Planetary Change*, **19**(1), 12–13.

Goosse, H., P. Y. Barriat, W. Lefebvre, M. F. Loutre, and V. Zunz, 2013: Introduction to climate dynamics and climate modeling. [Available online at http://www.climate.be/textbook.]

Graham, N., and Coauthors, 2007: Tropical Pacific –mid-latitude teleconnections in medieval times. *Climatic Change*, **83**(1), 241–285, doi: 10.1007/s10584-007-9239-2.

Guiot, J., and C. Corona, 2010: Growing season temperatures in Europe and climate forcings over the past 1400 years. *PloS one*, **5**(4), e9972, doi: 10.1371/journal.pone.0009972.

Hegerl, G., T. Crowley, S. Baum, K. Kim, and W. Hyde, 2003: Detection of volcanic, solar and greenhouse gas signals in paleoreconstructions of northern hemi-

spheric temperature. *Geophys. Res. Lett.*, **30**, doi: 10.1029/2002GL016635.

Hegerl, G., T. Crowley, M. Allen, W. Hyde, H. Pollack, J. Smerdon, and E. Zorita, 2007: Detection of human influence on a new, validated 1500-year temperature reconstruction. *J. Climate*, **20**, 650–666.

IPCC, 2007: *Climate Change 2007: The physical science basis. Contribution of Working Group I to the Fourth Assessment Report of the Intergovermental Panel on Climate Change*, S. Solomon et al., Eds., Cambridge University Press, Cambridge, United Kingdom and New York, NY, USA, 996pp.

Jansen, E., and Coauthors, 2007: Palaeoclimate. *Climate change 2007: The physical science basis. Contribution of Working Group I to the fourth assessment report of the intergovernmental panel on climate change*. Solomon et al., Eds, Cambridge University Press, Cambridge, 433-497.

Jin, X. Z., X. H. Zhang, and T. J. Zhou, 1999: Fundamental framework and experiments of the third generation of IAP/LASG world ocean general circulation model. *Adv. Atmos. Sci.*, **16**(2), 197–215.

Jones, P., and Coauthors, 2009: High-resolution palaeoclimatology of the last millennium: A review of current status and future prospects. *The Holocene*, **19**(1), 3–49.

Kiehl, J. T., 1994: On the observed near cancellation between longwave and shortwave cloud forcing in tropical regions. *J. Climate*, **7**(4), 559–565.

Knutson, T. R., and Coauthors, 2006: Assessment of twentieth-century regional surface temperature trends using the GFDL CM2 coupled models. *J. Climate*, **19**(9), 1624–1651.

Lee, W. H., S. F. Iacobellis, and R. C. J. Somerville, 1997: Cloud radiation forcings and feedbacks: General circulation model tests and observational validation. *J. Climate*, **10**(10), 2479–2496.

Li, L., B. Wang, Y. Wang, and W. Hui, 2007: Improvements in climate simulation with modifications to the Tiedtke convective parameterization in the grid-point atmospheric model of IAP LASG (GAMIL). *Adv. Atmos. Sci.*, **24**(2), 323–335, doi: 10.1007/s00376-007-0323-3.

Li, Z. X., and S. Conil, 2003: A 1000-year simulation with the IPSL ocean-atmosphere coupled model. *Annals of Geophysics*, **46**(1), 39–46.

Liu, H. L., X. H. Zhang, W. Li, Y. Q. Yu, and R. C. Yu, 2004: An eddy-permitting oceanic general circulation model and its preliminary evaluation. *Adv. Atmos. Sci.*, **21**(5), 675–690.

Liu, J., B. Wang, H. Wang, X. Kuang, and R. Ti, 2011: Forced response of the East Asian summer rainfall over the past millennium: Results from a coupled model simulation. *Climate Dyn.*, **36**(1), 323–336.

Mann, M. E., 2002: The value of multiple proxies. *Science,* **297**(5586), 1481–1482, doi: 10.1126/science.1074318.

Mann, M. E., and Coauthors, 2009: Global signatures and dynamical origins of the little ice age and medieval climate anomaly. *Science*, **326**(5957), 1256–1260, doi: 10.1126/science.1177303.

Man, W. M., and T. J. Zhou, 2011: Forced response of atmospheric oscillations during the last millennium simulated by a climate system model. *Chinese Science Bulletin*, **56**, 3042–3052.

Man, W. M., T. J. Zhou, J. Zhang, and B. Wu, 2011: The 20th century climate simulated by LASG/IAP climate system model FGOALS_gl. *Acta Meteorologica Sinica*, **69**(4), 644–654. (in Chinese)

Moberg, A., D. M. Sonechkin, K. Holmgren, N. M. Datsenko, and W. Karlen, 2005: Highly variable Northern Hemisphere temperatures reconstructed from low- and high-resolution proxy data. *Nature*, **433**(7026), 613–617.

Norris, J. R., 2005: Multidecadal changes in near-global cloud cover and estimated cloud cover radiative forcing. *J. Geophys. Res.,* **110**(D08206), doi: 10.1029/2004JD005600.

NRC (Natinal Research Council), 2006: *National Research Council Committee: Surface Temperature Reconstruction for the Last 2,000 Years*. National Academies Press, Washington, D.C., 145pp.

Peng, Y., Y. Xu, and L. Jin, 2009: Climate changes over eastern China during the last millennium in simulations and reconstructions. *Quaternary International*, **208**(1–2), 11–18, doi: 10.1016/j.quaint.2009.02.013.

Philander, S. G. H., D. Gu, D. Halpern, G. Lambert, N. C. Lau, T. Li, and R. C. Pacanowski, 1996: Why the ITCZ is mostly north of the equator. *J. Climate*, **9**(12), 2958–2972.

Phipps, S. J., 2010: The CSIRO Mk3L climate system v1.2. Tech. Rep. No. 4, Antarctic Climate & Ecosystems CRC, Hobart, Tasmania, Australia, 122pp.

Quaas, J., O. Boucher, J. L. Dufresne, and H. Le Trent, 2004: Impacts of greenhouse gases and aerosol direct and indirect effects on clouds and radiation in atmospheric GCM simulations of the 1930–1989 period. *Climate Dyn.*, **23**(7–8), 779–789.

Raddatz, T., and Coauthors, 2007: Will the tropical land biosphere dominate the climate–carbon cycle feedback during the 21st century? *Climate Dyn.*, doi: 10.1007/s00382-007-0247-8.

Schmidt, G. A., and Coauthors, 2006: Present day atmospheric simulations using GISS ModelE: Comparison to in-situ, satellite and reanalysis data. *J. Climate*, **19**, 153–192, doi: 10.1175/JCLI3612.1.

Schmidt, G., and Coauthors, 2011: Climate forcing reconstructions for use in PMIP simulations of the last millennium (v1.0), Geoscientific Model Development, **4**, 33–45, doi: 10.5194.gmd-4-33-2011.

Screen, J. A., and I. Simmonds, 2010: The central role of diminishing sea ice in recent Arctic temperature amplification. *Nature*, **464**(7293), 1334–1337.

Servonnat, J., P. Yiou, M. Khodri, D. Swingedouw, and S. Denvil, 2010: Influence of solar variability, CO2 and orbital forcing between 1000 and 1850 AD in the IPSLCM4 model. *Climate of the Past*, **6**(4), 445–460.

Steig, E. J., D. P. Schneider, S. D. Rutherford, M. E.

Mann, J. C. Comiso, and D. T. Shindell, 2009: Warming of the Antarctic ice-sheet surface since the 1957 international geophysical year. *Nature*, **457**(7228), 459–462, doi: 10.1038/nature07669.

Steinhilber, F., J. Beer, and C. Fröhlich, 2009: Total solar irradiance during the holocene. *Geophys. Res. Lett.*, **36**, doi: 10.1029/2009GL040142.

Stott, P. A., S. F. B. Tett, G. S. Jones, M. R. Allen, J. F. B. Mitchell, and G. J. Jenkins, 2000: External control of 20th century temperature by natural and anthropogenic forcings. *Science*, **290**(5499), 2133–2137.

Swingedouw, D., L. Terray, C. Cassou, A. Voldoire, D. Salas-Mélia, and J. Servonnat, 2011: Natural forcing of climate during the last millennium: Fingerprint of solar variability. *Climate Dyn.*, **36**(7), 1349–1364.

Tapping, K., D. Boteler, P. Charbonneau, A. Crouch, A. Manson, and H. Paquette, 2007: Solar magnetic activity and total irradiance since the Maunder Minimum. *Solar Physics*, **246**(2), 309–326.

Tett, S. F. B., P. A. Stott, M. R. Allen, W. J. Ingram, and J. F. B. Mitchell, 1999: Causes of twentieth-century temperature change near the Earth's surface. *Nature*, **399**(6736), 569–572.

Tett, S. F. B., and Coauthors, 2002: Estimation of natural and anthropogenic contributions to twentieth century temperature change. *J. Geophys. Res.*, **107**(D16), doi: 10.1029/2000JD000028.

Verleyen, E., and Coauthors, 2011: Post-glacial regional climate variability along the East Antarctic coastal margin—Evidence from shallow marine and coastal terrestrial records. *Earth-Science Reviews*, **104**(4), 199–212, doi: 10.1016/j.earscirev.2010.10.006.

Wang, S. W., Z. H. Xie, J. N. Cai, J. H. Zhu, and D. Y. Gong, 2002: Investigation of the global mean temperature changes during the past 1000 years. *Progress in Natural Science*, **12**, 1145–1149. (in Chinese)

Wen, X. Y., T. J. Zhou, S. W. Wang, B. Wang, H. Wan, and J. Li, 2007: Performance of a reconfigured atmospheric general circulation model at low resolution. *Adv. Atmos. Sci.*, **24**(4), 712–728, doi: 10.1007/s00376-007-0712-7.

Xin, X. G., T. W. Wu, J. L. Li, Z. Z. Wang, W. P. Li, and F. H. Wu, 2013: How well dose BCC_CSM1.1 reproduce the 20th century climate change over China? *Atmos. Oceanic Sci. Lett.*, **6**(1), 21–26.

Yu, R. C., M. H. Zhang, and R. D. Cess, 1999: Analysis of the atmospheric energy budget: A consistency study of available data sets. *J. Geophys. Res.*, **104**(D8), 9655–9661.

Zhang, J., T. Zhou, W. M. Man, and L. Li, 2009: The transient simulation of little ice age by LASG/IAP climate system model FGOALS_gl. *Quaternary Sciences*, **29**(6), 1125–1134. (in Chinese)

Zhou, T. J., B. Wu, X. Y. Wen, L. J. Li, and B. Wang, 2008: A fast version of LASG/IAP climate system model and its 1000-year control integration. *Adv. Atmos. Sci.*, **25**(4), 655–672, doi: 10.1007/s00376-008-0655-7.

Zhou, T. J., W. M. Man, and J. Zhang, 2009: Progress in numerical simulations of the climate over the last millennium *Advances in Earth Science*, **24**, 469–476. (in Chinese)

Zhou, T. J., B. Li, W. M. Man, L. X. Zhang, and J. Zhang, 2011: A comparison of the medieval warm period, little ice age and 20th century warming simulated by the FGOALS climate system model. *Chinese Science Bulletin*, **56**, 3028–3041.

Zebiak, S. E., and M. A. Cane, 1987: A model El Niño-Southern Oscillation. *Mon. Wea. Rev.*, **115**, 2262–2278.